

# Signal in the noise: temporal variation in exponentially growing populations

Eric W. Jones<sup>1,\*</sup>, Joshua Derrick<sup>2</sup>, Roger M. Nisbet<sup>3</sup>, Will Ludington<sup>2,4</sup>, and David A. Sivak<sup>1</sup>

<sup>1</sup>Department of Physics, Simon Fraser University

<sup>2</sup>Department of Embryology, Carnegie Institution for Science

<sup>3</sup>Department of Ecology, Evolution, and Marine Biology, University of California, Santa Barbara and

<sup>4</sup>Department of Biology, Johns Hopkins University

(Dated: April 28, 2023)

In exponential population growth, intrinsic variability in the timing of individual division events compounds to produce variable macroscopic outcomes. For a stochastic model of exponential growth, we derive a power-law relationship that relates noise in the macroscopic outcomes to growth rate and inoculum size. Population-growth experiments in *E. coli* and *S. aureus* with inoculum sizes ranging between 1 and 100 are consistent with this relationship. Noise encodes (and can be used to deduce) information about the early growth rate of a population.

Bacteria divide, viruses replicate, and yeast cells bud, leading (if unimpeded) to exponential growth. Since division events are generally not evenly separated in time, even identically prepared systems will give rise to different growth trajectories. The simple birth process is perhaps the most basic stochastic model of exponential growth: it assumes that each individual divides according to a Poisson process. This model was first solved in 1939 to describe the exponential growth of neutrons in nuclear fission [1, 2], then subsequently used as an analytically tractable model of bacterial growth [3]. Since then, age-structured population-growth models that account for an organism's life history have been proposed [4–9] and empirically characterized with high-throughput microscopy [10–13].

Traditionally, treatments of these population-growth models have maintained a focus on population abundance, for example quantifying a population's noise by the coefficient of variation of the abundance [14, 15]. In this Letter we offer an alternative approach by characterizing noisy population growth in terms of a population's temporal variation, quantified by the *temporal standard deviation* (TSD), the standard deviation of the distribution of times at which an exponentially growing population first hits a threshold number. Specifically, we apply stochastic models of exponential growth to relate the TSD at large thresholds to the inoculum size, deriving a power-law relationship that matches direct experimental tests in *Escherichia coli* and *Staphylococcus aureus*. Reformulating the canonical system of exponential growth in terms of temporal variation naturally leads to analytic and practical insights, with implications for a plethora of exponentially growing populations.

As a tangible example, consider milk spoilage [17–19]. Milk spoilage occurs when the exponential growth of a contaminant bacteria reaches some threshold population density. In a refrigerator at 5°C, the common bacterial contaminant *Listeria monocytogenes* divides every ~17 hours [20]. It is straightforward to measure the distribution of times at which a number of identically prepared

containers of milk spoil: if properly refrigerated, pasteurized milk has a shelf life (time to reach a bacterial concentration of 20,000 CFU/mL [21]) ranging from 10 to 21 days post processing [16]. Figure 1 shows simulated abundance trajectories for a simple birth process modeling the growth of *L. monocytogenes*, which indicate that a liter of milk inoculated by a single bacterium has a shelf life of roughly 17 days with a 3.7-day range, while a liter of milk inoculated by 100 bacteria has a shelf life of 12 days with a 0.3-day range. Nearly 4 days of the variation in the timing of milk spoilage can there-

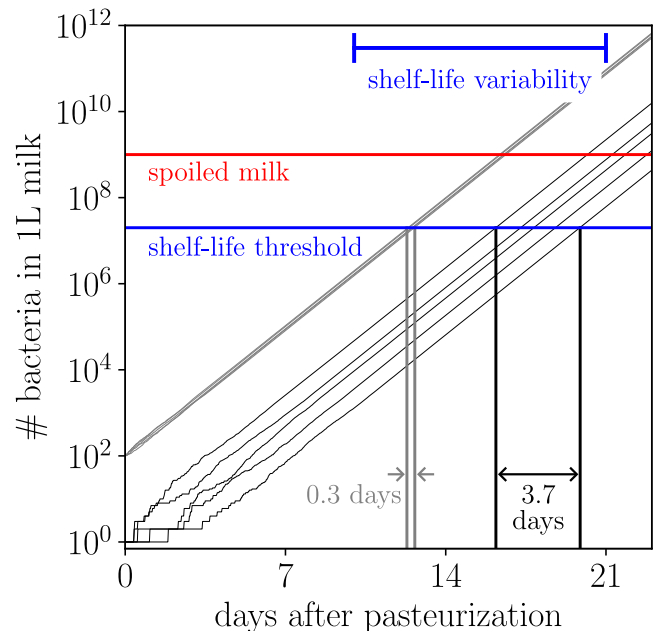


FIG. 1. **Intrinsic variability contributes to the reported 11-day variation in the shelf life of milk.** Abundance trajectories from a simple birth process modeling the growth of *L. monocytogenes*, a common milk contaminant that divides roughly every 17 hours, inoculated with a single individual (black) or 100 individuals (gray). The spread of these trajectories is quantified by the temporal standard deviation [Eq. (10a)]. The empirical shelf-life variability of 10-21 days is reported in [16].

\* eric\_jones\_2@sfu.ca

fore be attributed to intrinsic variability, at least for the simple birth process. By decomposing variability into its constitutive processes, food-processing engineers can learn whether variability is inevitable or whether it can be mitigated.

*Model description and solution.*—Consider a simple birth process in which each individual divides according to a Poisson process with rate  $\mu$ . For a population of  $n$  individuals, the probability  $B_n$  per unit time that an individual will divide (conventionally the “birth rate” in Markov-process literature [22]) is

$$B_n = \mu n. \quad (1)$$

The probability  $P_t(n | n_0)$  that the population consists of  $n$  individuals at time  $t$ , given an initial condition of  $n_0$  individuals, is governed by the master equation

$$\frac{d}{dt} P_t(n | n_0) = \mu(n-1)P_t(n-1 | n_0) - \mu n P_t(n | n_0). \quad (2)$$

In  $P_t(n | n_0)$ ,  $n$  is the random variable with normalization  $\sum_{n=0}^{\infty} P_t(n | n_0) = 1$ . Using generating functions [1, 3], the solution is

$$P_t(n | n_0) = \frac{(n-1)!}{(n_0-1)!(n-n_0)!} e^{-\mu n_0 t} (1 - e^{-\mu t})^{n-n_0}. \quad (3)$$

The first two cumulants are the average abundance

$$\langle n \rangle = n_0 e^{\mu t}, \quad (4)$$

and the variance

$$\langle (n - \langle n \rangle)^2 \rangle = n_0 e^{\mu t} (e^{\mu t} - 1). \quad (5)$$

*Calculating the temporal standard deviation.*—The first-passage-time distribution  $P_n^{\text{FP}}(t | n_0)$  is the distribution of times at which a population with inoculum size  $n_0$  first reaches  $n$  individuals.  $P_n^{\text{FP}}(t | n_0)$  can be solved using the renewal equation

$$P_t(n | n_0) = \int_0^t P_{t'}(n | n) P_n^{\text{FP}}(t - t' | n_0) dt' \quad (6)$$

and Laplace-transform methods (Supplementary Information, Section A):

$$P_n^{\text{FP}}(t | n_0) = \mu n \binom{n-1}{n_0-1} \times \sum_{i=0}^{n-n_0} \binom{n-n_0}{i} (-1)^i \left(1 - \frac{n_0+i}{n}\right) e^{-\mu(n_0+i)t}. \quad (7)$$

The probability that in a small time  $t$  no organisms divide is  $(1 - \mu t)^n$ , so the probability that at least one of the  $n$  organisms divides becomes almost a certainty for  $n \gg 1/(\mu t)$ , leading to  $P_t(n | n) \approx \delta(t)/(\mu n)$  for Dirac delta function  $\delta(t)$ : in this limit,  $P_n^{\text{FP}}(t | n_0) \approx \mu n P_t(n | n_0)$ .

The mean first-passage time  $\langle t \rangle_{n | n_0}$  to reach threshold  $n$  starting from  $n_0$  individuals is (SI, Section B)

$$\langle t \rangle_{n | n_0} = \frac{1}{\mu} \left( \frac{1}{n_0} + \frac{1}{n_0+1} + \cdots + \frac{1}{n-1} \right), \quad (8a)$$

$$\approx \frac{\ln n}{\mu} \quad \text{for large } n \gg n_0. \quad (8b)$$

The *temporal variance*  $\sigma_t^2 \equiv \langle (t - \langle t \rangle)^2 \rangle_{n | n_0}$  is (SI, Section B)

$$\sigma_t^2 = \frac{1}{\mu^2} \left[ \frac{1}{n_0^2} + \frac{1}{(n_0+1)^2} + \cdots + \frac{1}{(n-1)^2} \right], \quad (9)$$

and therefore the *temporal standard deviation* is

$$\sigma_t = \frac{1}{\mu} \left[ \frac{1}{n_0^2} + \frac{1}{(n_0+1)^2} + \cdots + \frac{1}{(n-1)^2} \right]^{1/2} \quad (10a)$$

$$\approx \frac{1}{\mu n_0^{1/2}} \quad \text{for large } n \gg n_0. \quad (10b)$$

This is our main theoretical result: a simple relationship between TSD, growth rate, and inoculum size that is in complete accordance—as we will show—with bacterial population-growth experiments. An alternative and approximate derivation of Eq. (9), provided in the Supplementary Information Section C, calculates how an abundance distribution transforms under deterministic exponential growth. In Eqs. (8a) and (9), the explicit contributions of each population size from  $n_0$  to  $n-1$ , itemized term by term, reflect the Markovian (memoryless) dynamics:

$$\langle t \rangle_{n | n_0} = \sum_{i=n_0}^{n-1} \langle t \rangle_{i+1 | i} = \sum_{i=n_0}^{n-1} \frac{1}{\mu i}, \quad (11a)$$

$$\langle (t - \langle t \rangle)^2 \rangle_{n | n_0} = \sum_{i=n_0}^{n-1} \langle (t - \langle t \rangle)^2 \rangle_{i+1 | i} = \sum_{i=n_0}^{n-1} \frac{1}{(\mu i)^2}. \quad (11b)$$

*Growth experiments in bacteria.*—To empirically test the predicted TSDs of exponentially growing populations, we measured the growth of *E. coli* and *S. aureus*. At least 30 biological replicates were prepared for each inoculum size and grown over one or two days. Inoculum sizes were set by pipetting a dilute solution of bacteria growing in mid-log phase into a 96-well plate. Spot plating the same volume of this dilute solution confirmed that the inoculum size was Poisson distributed (Fig. S1). Bacterial abundance was inferred by measuring the optical density of each well every 2 minutes.

Figures 2a and 2b show representative subsets of abundance trajectories for *E. coli* and *S. aureus*, respectively. Bacteria grow exponentially until they reach an optical density of  $\sim 0.2$ , then grow more slowly until they reach carrying capacity. During the exponential-growth

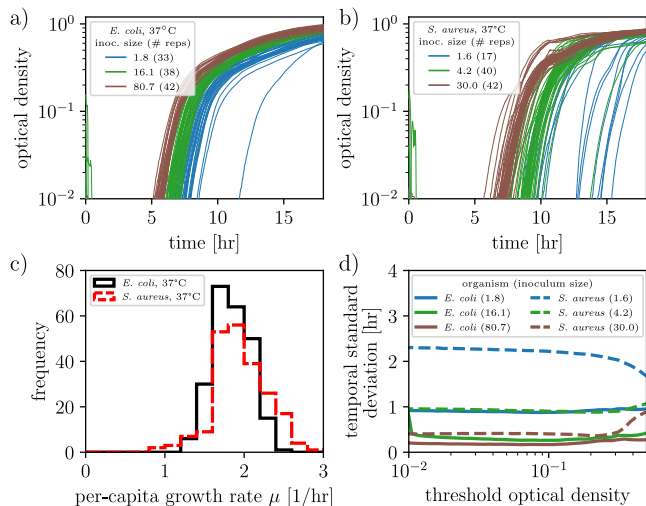


FIG. 2. **Empirical analyses of bacterial growth trajectories.** (a, b) Measured abundance trajectories in *E. coli* and *S. aureus* as functions of time for different mean inoculum sizes. (c) Distribution of log-phase growth rates pooled across replicates and inoculum sizes, evaluated at an optical density of 0.03 (SI Methods). (d) Temporal standard deviations as functions of threshold optical density for different mean inoculum sizes.

phase, each individual’s division rate is  $\sim 2$ /hour ( $\sim 20$ – $30$ -minute division times). Figure 2c shows the distribution of growth rates across replicates, calculated as the slope of the log-transformed optical-density time series evaluated at a threshold optical density of 0.03 (SI Methods). Measuring the growth rate  $\mu$  at an optical density of 0.02 increases its value by 15%, while evaluating it at 0.05 decreases its value by 10%. Equation (10a) predicts that the temporal standard deviation for the first-passage time to threshold  $n$  asymptotes to a constant value for  $n \gtrsim 50$ . Figure 2d confirms this prediction: the TSD is approximately the same for threshold optical densities 0.01–0.3 (corresponding to hundreds of thousands to millions of bacteria).

Bacterial growth experiments were performed for 35 inoculum sizes, yielding 1,381 total growth curves. Figure 3 shows how TSDs depend on inoculum size in units of hours (inset) and in units of division times (main figure). An organism’s division time is defined as  $\ln(2)/\mu$  for division rate  $\mu$ : at 37°C, *E. coli* and *S. aureus* have division times of  $\sim 22$  minutes, and at 25°C *E. coli* has a division time of  $\sim 52$  minutes (SI Methods). Presenting the data in terms of division times rather than hours collapses the TSDs of *E. coli* at 25°C onto the TSDs of *E. coli* at 37°C in Fig. 3.

In the simple birth process, stochasticity is generated exclusively by variability in the timing of division events. Since additional extrinsic sources of noise (like temperature fluctuations or variable media conditions) are not included in the simple birth process, we hypothesized that the simple birth process would underestimate the noise in the empirical measurements. This hypothesis amounts

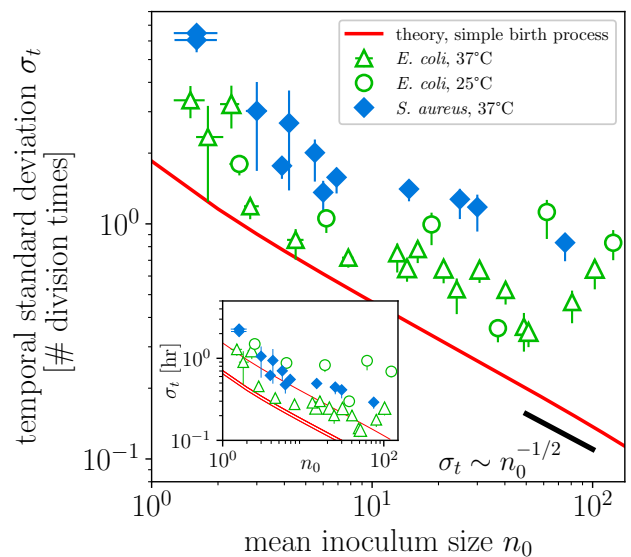


FIG. 3. **Temporal standard deviation scales inversely with the square root of the inoculum size.** Temporal standard deviations for a total of 35 inoculum sizes in *E. coli* and *S. aureus*, in units of division times (at least 15 replicates per inoculum size, average 40) (SI Methods). (inset) TSDs plotted in units of hours. Error bars indicate 68% confidence intervals of the mean (SI Methods). The theoretical relationship between TSD and inoculum size [red line, Eq. (10a)] derived for the simple birth process (not a fit) lies under every single data point. (inset) Red lines from top to bottom calculated with growth rates from *E. coli* at 25°C, *E. coli* at 37°C, and *S. aureus* at 37°C. As hypothesized, population-growth experiments were consistently noisier than the simple birth process limit.

to a prediction that, on net, the factors not captured by the simple birth process that increase the noise (*e.g.*, extrinsic noise and Poisson-distributed inocula) dominate those that decrease it (*e.g.*, age-structured growth). This hypothesis is borne out by the data: the temporal standard deviation predicted by the simple birth process (red line) lies below all 35 experimentally tested inoculum sizes (colorful symbols). Figure 3, our main empirical result, provides strong experimental support for the relationship [Eq. (10a)] as a bound.

*Growth-rate inference from TSD and inoculum size.*—By inverting Eq. (10a) relating TSD and inoculum size, a lower-bound  $\mu_{\text{LB}}$  for the growth rate can be inferred by growing replicate cultures with inoculum size  $n_0$  and calculating the TSD:

$$\mu_{\text{LB}} = \frac{1}{\sigma_t} \left[ \frac{1}{n_0^2} + \frac{1}{(n_0 + 1)^2} + \dots + \frac{1}{(n - 1)^2} \right]^{1/2}. \quad (12)$$

This meets an important need in microbial ecology experiments, which is to measure the growth rate of strains before they significantly change the media. Figure S2a compares these inferred growth-rate lower bounds, taken over all inoculum sizes, to the directly measured growth

rates. For all three combinations of organism and growth condition, the inferred growth rate indeed lower bounds the measured growth rate: the measured rate exceeded the lower bound by 3% in *E. coli* at 37°C, 51% in *E. coli* at 25°C, and 95% in *S. aureus* at 37°C. For exponentially growing populations in which the growth rate itself varies stochastically [23, 24] (*e.g.*, due to environmental fluctuations), the long-run growth rate underestimates the mean growth rate; in this case, the inferred lower bound (12) of the growth rate is especially conservative.

We used simulations of the simple birth process to probe how confidence in the estimation of  $\mu$  depends on the number of replicate growth trajectories. Fig. S2b shows that with  $\sim 40$  replicate trajectories, the growth rate can be inferred to within 10% of its true value.

*Beyond the simple birth process.*—A number of simplifying assumptions must be made in order to model bacterial growth as a simple birth process. Next, we sequentially relax these assumptions to investigate more biologically faithful models.

First, bacterial inoculation in our experiments—performed by pipetting a fixed volume of a dilute solution of bacteria—resulted in Poisson-distributed inocula (Fig. S1). Populations with Poisson-distributed inocula are more variable than populations that are exactly inoculated, as variability in the inoculum size propagates through the growth dynamics. The temporal spread due solely to the Poisson inoculation and in the absence of intrinsic noise—when growth dynamics follow a deterministic exponential curve—is comparable to the spread due to intrinsic noise in a simple birth process with exact inoculation (Fig. S3). In fact, the relationship between TSD and inoculum size for a system with Poisson-distributed inocula and no intrinsic noise (SI, Section D) is, to leading order, the same as for the simple birth process with intrinsic noise and exact inoculation [Eq. (10b)].

Second, bacterial division is precisely orchestrated, yet the simple birth process approximates it as a memoryless process. To account for the structure of bacterial division, we examined a deterministic, non-Markovian model of age-structured bacterial growth (SI, Section E). Kendall first explored these models in detail and demonstrated that a tighter division-time distribution produces a tighter spread of growth trajectories [3].

In such age-structured population models, division events that are initially synchronized across a population will desynchronize over time, until eventually the growth dynamics of the population as a whole are indistinguishable from those of the Poissonian simple birth process [25]. For a division-time distribution that mimics *E. coli*'s—with 25-minute average division time and 22% coefficient of variation [3]—the growth dynamics of a single inoculum will asymptote to pure exponential growth after  $\sim 3$  division cycles (Fig. S4) [26]. In our bacterial growth experiments, TSDs are evaluated at a threshold optical density of 0.03, by which time 10-20 division cycles have occurred. Thus, abundance oscillations predicted by age-structured growth models cannot

be resolved with these optical-density measurements.

Third, we performed stochastic simulations of bacterial growth that account for both Poisson-distributed inocula and age-structured division-time distributions (SI Methods). We found TSDs depend on inoculum size in a qualitatively similar way for both the simple birth process with exact inoculation and for an age-structured model with Poisson-distributed inocula (Fig. S3).

We conclude that in this instance, the simple birth process is sufficient to capture the empirically observed variability in exponentially growing populations. Moreover, the simple birth process is analytically tractable, enabling direct calculation of the cumulants of the first-passage-time distribution [Eq. (11)] and quantitatively revealing the rate at which variation accumulates in a growing population. Namely, the temporal variance reaches half of its asymptotic value after a single division time (SI, Section C), and the contributions to the temporal variance fall off as the inverse square of the population size. This trend is also observed in age-structured population-growth models (Fig. S5). We conjecture that these properties hold for a general class of exponentially growing populations.

*Discussion*—Stochastic population growth, by its nature, produces a distribution of abundance trajectories over time [27]. For exponentially growing populations, the mean trajectory of this distribution contains information about the population growth rate, given by the slope of the log-transformed trajectory. We demonstrated in this Letter that the temporal variance is a second statistic that reports on the population growth rate. Temporal variation is especially informative when population size increases monotonically; a significant death rate complicates the situation (*e.g.*, populations can go extinct) [22].

Since the largest contributions to the noise occur at small population sizes, the growth rate at small population sizes is made manifest in the noise. If the growth rate changes as a population grows (with negligibly few deaths), then the contributions to the temporal variance are dominated by terms involving the initial growth rate. Thus, while the mean abundance trajectory reveals the instantaneous growth rate when it is measured, the temporal variance reflects the initial growth rate. Traditionally it has been difficult to measure the growth rate of bacteria at small population sizes without expensive microscopy equipment, since conventional optical-density measurements are unable to resolve growth at small scales [28]. Temporal variation, on the other hand, is straightforward to empirically measure.

There are a number of applications where temporal variation is relevant. Microbiologists can calibrate their instruments by measuring the TSDs of a set of bacterial replicates and comparing them to the lower bound predicted by Eq. (10b), reminiscent of other fluctuation-based calibration methods [29]. Methicillin-resistant *S. aureus* (MRSA) is a virulent hospital pathogen, and we found that the noise in *S. aureus* growth was lower-bounded by the noise predicted by the simple birth pro-

cess, suggesting a lower bound on the standard deviation of the times at which patients develop MRSA symptoms following exposure. In a food-processing plant, the temporal standard deviation of a food's spoilage and the growth rate of the contaminant bacteria together suggest a lower bound on the inoculum size of the bacterial contaminant, from which the contamination source could be deduced.

A signal in the noise can be revealed when biological systems are modeled as stochastic processes [30]. For example, we have shown that information about early growth conditions is imprinted in the subsequent variation of exponentially growing populations. Noise is valu-

---

able, and provides another dimension in which insights may be inferred.

*Acknowledgements*—We thank Robert Scheffler and Ferdinand Pfab for helpful discussions. Support was provided by Banting and Pacific Institute for the Mathematical Sciences Postdoctoral Fellowships (E.W.J.); National Science Foundation IOS 2032985 (W.L.); Natural Sciences and Engineering Research Council of Canada (NSERC) Discovery Grant and a Tier-II Canada Research Chair (D.A.S.); and the Carnegie-Canada Foundation (W.L. and D.A.S.).

**Supplementary Information**  
**Signal in the noise: temporal variation in exponentially growing populations**

**CONTENTS**

|  |    |
|--|----|
| Section A: Exact first-passage-time calculation via the renewal equation                         | 7  |
| Section B: Mean and variance of the first-passage-time distribution for the simple birth process | 8  |
| Section C: Abundance-based derivation for relationship between TSD and inoculum size             | 10 |
| Section D: Relationship between TSD and inoculum size for Poisson-distributed inocula            | 12 |
| Section E: Deterministic age-structured population growth  | 15 |
| Methods  | 19 |
| References   | 21 |

## SECTION A: EXACT FIRST-PASSAGE-TIME CALCULATION VIA THE RENEWAL EQUATION

The probability  $P_t(n|n_0)$  of a population consisting of  $n$  individuals at time  $t$  given there were initially  $n_0$  individuals and the first-passage-time distribution  $P_n^{\text{FP}}(t|n_0)$  of times  $t$  at which an abundance trajectory first reaches  $n$  individuals given there were initially  $n_0$  individuals are related by the renewal equation [31],

$$P_t(n|n_0) = \int_0^t P_{t'}(n|n) P_n^{\text{FP}}(t-t'|n_0) dt'. \quad (\text{S1})$$

For the simple birth process, the general solution  $P_t(n|n_0)$  is given by Eq. (3),

$$P_t(n|n_0) = \frac{(n-1)!}{(n_0-1)!(n-n_0)!} e^{-\mu n_0 t} (1 - e^{-\mu t})^{n-n_0} \quad (\text{S2a})$$

$$= \binom{n-1}{n_0-1} e^{-\mu n_0 t} (1 - e^{-\mu t})^{n-n_0}, \quad (\text{S2b})$$

and the probability of remaining at state  $n$  for at least time  $t'$  is

$$P_{t'}(n|n) = e^{-\mu n t'}. \quad (\text{S3})$$

Laplace transforms can be used to solve Eq. (S1) for the first-passage-time distribution  $P_n^{\text{FP}}(t|n_0)$ . The Laplace transform  $\hat{P}_s(n|n_0) \equiv \mathcal{L}[P_t(n|n_0)]$  of the simple-birth-process solution is

$$\hat{P}_s(n|n_0) = \int_0^\infty P_t(n|n_0) e^{-ts} dt \quad (\text{S4a})$$

$$= \binom{n-1}{n_0-1} \int_0^\infty e^{-\mu n_0 t} (1 - e^{-\mu t})^{n-n_0} e^{-ts} dt \quad (\text{S4b})$$

$$= \binom{n-1}{n_0-1} \int_0^\infty \sum_{i=0}^{n-n_0} \binom{n-n_0}{i} (-1)^i e^{-t(\mu n_0 + \mu i + s)} dt \quad (\text{S4c})$$

$$= \binom{n-1}{n_0-1} \sum_{i=0}^{n-n_0} \binom{n-n_0}{i} (-1)^i \frac{1}{\mu(n_0 + i) + s}. \quad (\text{S4d})$$

Also,

$$\hat{P}_s(n|n) = \frac{1}{s + \mu n}. \quad (\text{S5})$$

Then, by the convolution theorem,  $\mathcal{L}\left[\int_0^t f(t)g(t-t')dt'\right] = \hat{f}(s)\hat{g}(s)$ ,

$$\hat{P}_n^{\text{FP}}(s|n_0) = \binom{n-1}{n_0-1} \sum_{i=0}^{n-n_0} \binom{n-n_0}{i} (-1)^i \left[1 + \frac{\mu n - \mu(n_0 + i)}{s + \mu(n_0 + i)}\right] \quad (\text{S6a})$$

$$= \binom{n-1}{n_0-1} \sum_{i=0}^{n-n_0-1} \binom{n-n_0}{i} (-1)^i \frac{\mu n - \mu(n_0 + i)}{s + \mu(n_0 + i)}, \quad (\text{S6b})$$

where the last equality is because the sum of binomial coefficients with alternating sign vanishes. Inverting the transform gives

$$P_n^{\text{FP}}(t|n_0) = \mu n \binom{n-1}{n_0-1} \sum_{i=0}^{n-n_0} \binom{n-n_0}{i} (-1)^i \left(1 - \frac{n_0 + i}{n}\right) e^{-\mu(n_0 + i)t}. \quad (\text{S7})$$

This first-passage-time distribution may be compared to Eq. (S2b) with the binomial term expanded:

$$P_t(n|n_0) = \binom{n-1}{n_0-1} \sum_{i=0}^{n-n_0} \binom{n-n_0}{i} (-1)^i e^{-\mu(n_0 + i)t}. \quad (\text{S8})$$

Equation (S7) contains a factor  $1 - (n_0 + i)/n$  in each term of the summation, while Eq. (S8) does not. For small  $i$  the exponential factor does not vanish and scales as  $1/n$ , while for large  $i$  the exponential factor vanishes. In total,  $\mu n P_t(n|n_0)$  approximates  $P_n^{\text{FP}}(t|n_0)$  with an error that scales as  $1/n$ .

**SECTION B: MEAN AND VARIANCE OF THE FIRST-PASSAGE-TIME DISTRIBUTION FOR THE SIMPLE BIRTH PROCESS**

The mean first-passage time is

$$\langle t \rangle_{n|n_0} = \int_0^\infty t P_n^{\text{FP}}(t|n_0) dt \quad (\text{S9a})$$

$$= \mu n \binom{n-1}{n_0-1} \sum_{i=0}^{n-n_0} \left[ \binom{n-n_0}{i} (-1)^i \left(1 - \frac{n_0+i}{n}\right) \int_0^\infty t e^{-\mu(n_0+i)t} dt \right] \quad (\text{S9b})$$

$$= \frac{(n-n_0)\binom{n-1}{n_0-1}}{\mu} \left\{ \sum_{i=0}^{n-n_0} \left[ \binom{n-n_0}{i} \frac{(-1)^i}{(n_0+i)^2} \right] + \sum_{j=0}^{n-n_0-1} \left[ \binom{n-n_0-1}{j} \frac{(-1)^j}{(n_0+1+j)^2} \right] \right\}. \quad (\text{S9c})$$

Starting from the identity [32]

$$\sum_{k=0}^n \binom{n}{k} \frac{(-1)^k}{k+x} = \left[ x \binom{n+x}{n} \right]^{-1}; \quad (\text{S10})$$

differentiating with respect to  $x$  yields

$$-\sum_{k=0}^n \binom{n}{k} \frac{(-1)^k}{(k+x)^2} = \frac{d}{dx} \left[ \frac{n!}{x(x+1)\cdots(x+n)} \right] \quad (\text{S11a})$$

$$= -\frac{n!}{x(x+1)\cdots(x+n)} \left( \frac{1}{x} + \frac{1}{x+1} + \cdots + \frac{1}{x+n} \right). \quad (\text{S11b})$$

Therefore,

$$\langle t \rangle_{n|n_0} = \frac{n-n_0}{\mu n} \left( \frac{1}{n_0} + \frac{1}{n_0+1} + \cdots + \frac{1}{n} \right) + \frac{n_0}{\mu n} \left( \frac{1}{n_0+1} + \frac{1}{n_0+2} + \cdots + \frac{1}{n} \right) \quad (\text{S12})$$

$$= \frac{1}{\mu} \left( \frac{1}{n_0} + \frac{1}{n_0+1} + \cdots + \frac{1}{n-1} \right). \quad (\text{S13})$$

The variance  $\sigma_t^2 \equiv \langle t^2 \rangle_{n|n_0} - \langle t \rangle_{n|n_0}^2$  of the first-passage time distribution depends on the quantity

$$\langle t^2 \rangle_{n|n_0} = \int_0^\infty t^2 P_n^{\text{FP}}(t|n_0) dt \quad (\text{S14a})$$

$$= \mu n \binom{n-1}{n_0-1} \sum_{i=0}^{n-n_0} \left[ \binom{n-n_0}{i} (-1)^i \left(1 - \frac{n_0+i}{n}\right) \int_0^\infty t^2 e^{-\mu(n_0+i)t} dt \right] \quad (\text{S14b})$$

$$= \frac{2(n-n_0)\binom{n-1}{n_0-1}}{\mu^2} \left\{ \sum_{i=0}^{n-n_0} \left[ \binom{n-n_0}{i} \frac{(-1)^i}{(n_0+i)^3} \right] + \sum_{j=0}^{n-n_0-1} \left[ \binom{n-n_0-1}{j} \frac{(-1)^j}{(n_0+1+j)^3} \right] \right\} \quad (\text{S14c})$$

Differentiating again the identity in Eq. (S11) gives

$$2 \sum_{k=0}^n \binom{n}{k} \frac{(-1)^k}{(k+x)^3} = \frac{d^2}{dx^2} \left[ \frac{n!}{x(x+1)\cdots(x+n)} \right] \quad (\text{S15a})$$

$$= \frac{n!}{x(x+1)\cdots(x+n)} \left( \frac{1}{x} + \frac{1}{x+1} + \cdots + \frac{1}{x+n} \right)^2 \quad (\text{S15b})$$

$$+ \frac{n!}{x\cdots(x+n)} \left( \frac{1}{x^2} + \frac{1}{(x+1)^2} + \cdots + \frac{1}{(x+n)^2} \right). \quad (\text{S15c})$$

Therefore,

$$\langle t^2 \rangle_{n|n_0} = \frac{(n-n_0)}{\mu^2 n} \left[ \left( \frac{1}{n_0} + \frac{1}{n_0+1} + \cdots + \frac{1}{n} \right)^2 + \frac{1}{n_0^2} + \frac{1}{(n_0+1)^2} + \cdots + \frac{1}{n^2} \right] \quad (\text{S16a})$$

$$+ \frac{n_0}{\mu^2 n} \left[ \left( \frac{1}{n_0+1} + \frac{1}{n_0+2} + \cdots + \frac{1}{n} \right)^2 + \frac{1}{(n_0+1)^2} + \frac{1}{(n_0+2)^2} + \cdots + \frac{1}{n^2} \right]$$

$$= \frac{1}{\mu^2} \left[ \left( \sum_{q=n_0}^n \frac{1}{q} \right)^2 + \sum_{q=n_0}^n \frac{1}{q^2} - \frac{2}{n} \sum_{q=n_0}^n \frac{1}{q} \right]. \quad (\text{S16b})$$

Furthermore,

$$\langle t \rangle_{n|n_0}^2 = \frac{1}{\mu^2} \left( \sum_{q=n_0}^{n-1} \frac{1}{q} \right)^2. \quad (\text{S17})$$

Hence the variance  $\sigma_t^2$  is

$$\sigma_t^2 = \frac{1}{\mu^2} \left[ \left( \sum_{q=n_0}^n \frac{1}{q} \right)^2 + \sum_{q=n_0}^n \frac{1}{q^2} - \frac{2}{n} \sum_{q=n_0}^n \frac{1}{q} - \left( \sum_{q=n_0}^{n-1} \frac{1}{q} \right)^2 \right] \quad (\text{S18a})$$

$$= \frac{1}{\mu^2} \sum_{q=n_0}^{n-1} \frac{1}{q^2} \quad (\text{S18b})$$

$$= \frac{1}{\mu^2} \left[ \frac{1}{n_0^2} + \frac{1}{(n_0+1)^2} + \cdots + \frac{1}{(n-1)^2} \right]. \quad (\text{S18c})$$

**SECTION C: ABUNDANCE-BASED DERIVATION FOR RELATIONSHIP BETWEEN TSD AND INOCULUM SIZE**

For an initial population of  $n_0$  individuals growing exponentially in a deterministic manner, the time  $\tilde{t}$  at which this population will reach a threshold  $\Omega$  of individuals is

$$\tilde{t} = \frac{1}{\mu} \ln(\Omega/n_0). \quad (\text{S19})$$

We consider a generalization  $T(N)$  of this function in which the inoculum size is a random variable  $N$  rather than a fixed number  $n_0$ ,

$$T(N) = \frac{1}{\mu} \ln(\Omega/N), \quad (\text{S20})$$

which yields the distribution of first-passage times at a threshold  $\Omega$  assuming deterministic exponential growth. The mean and variance of the random variable  $T(N)$  can be Taylor expanded [33]:

$$\langle T(N) \rangle = T(\langle N \rangle) + \frac{T''(\langle N \rangle)}{2} [\langle N^2 \rangle - \langle N \rangle^2] + \text{higher-order terms}, \quad (\text{S21a})$$

$$\langle T(N)^2 \rangle - \langle T(N) \rangle^2 = [T'(\langle N \rangle)]^2 [\langle N^2 \rangle - \langle N \rangle^2] + \text{higher-order terms}, \quad (\text{S21b})$$

where the higher-order terms depend on higher cumulants of  $N$  and vanish when  $N$  is normally distributed.

Consider a random variable  $N(t)$  whose distribution is given by a solution of the simple birth process at time  $t$  with inoculum size  $n_0$ . Furthermore, consider a limit in which the threshold  $\Omega$  is much larger than the mean abundance  $\langle N(t) \rangle$ . Substituting the mean  $\langle N(t) \rangle = n_0 e^{\mu t}$  and variance  $\langle N(t)^2 \rangle - \langle N(t) \rangle^2 = n_0 e^{\mu t} (e^{\mu t} - 1)$  [from Eqs. (4) and (5)] into Eqs. (S21a) and (S21b) yields

$$\langle T(N(t)) \rangle = \frac{\ln(\Omega/(n_0 e^{\mu t}))}{\mu} + \frac{1 - e^{-\mu t}}{2\mu n_0} + O\left(\frac{1}{n_0^2}\right), \quad (\text{S22a})$$

$$\langle T(N(t))^2 \rangle - \langle T(N(t)) \rangle^2 = \frac{1}{\mu^2 n_0} (1 - e^{-\mu t}) + O\left(\frac{1}{n_0^2}\right), \quad (\text{S22b})$$

which for large  $t$  recovers to leading order the relationship between temporal variance and inoculum size for the simple birth process, Eq. (9). This formulation makes explicit the time scale over which variation is accumulated: half of the asymptotic temporal variance is accumulated after a single division time  $\ln(2)/\mu$ .

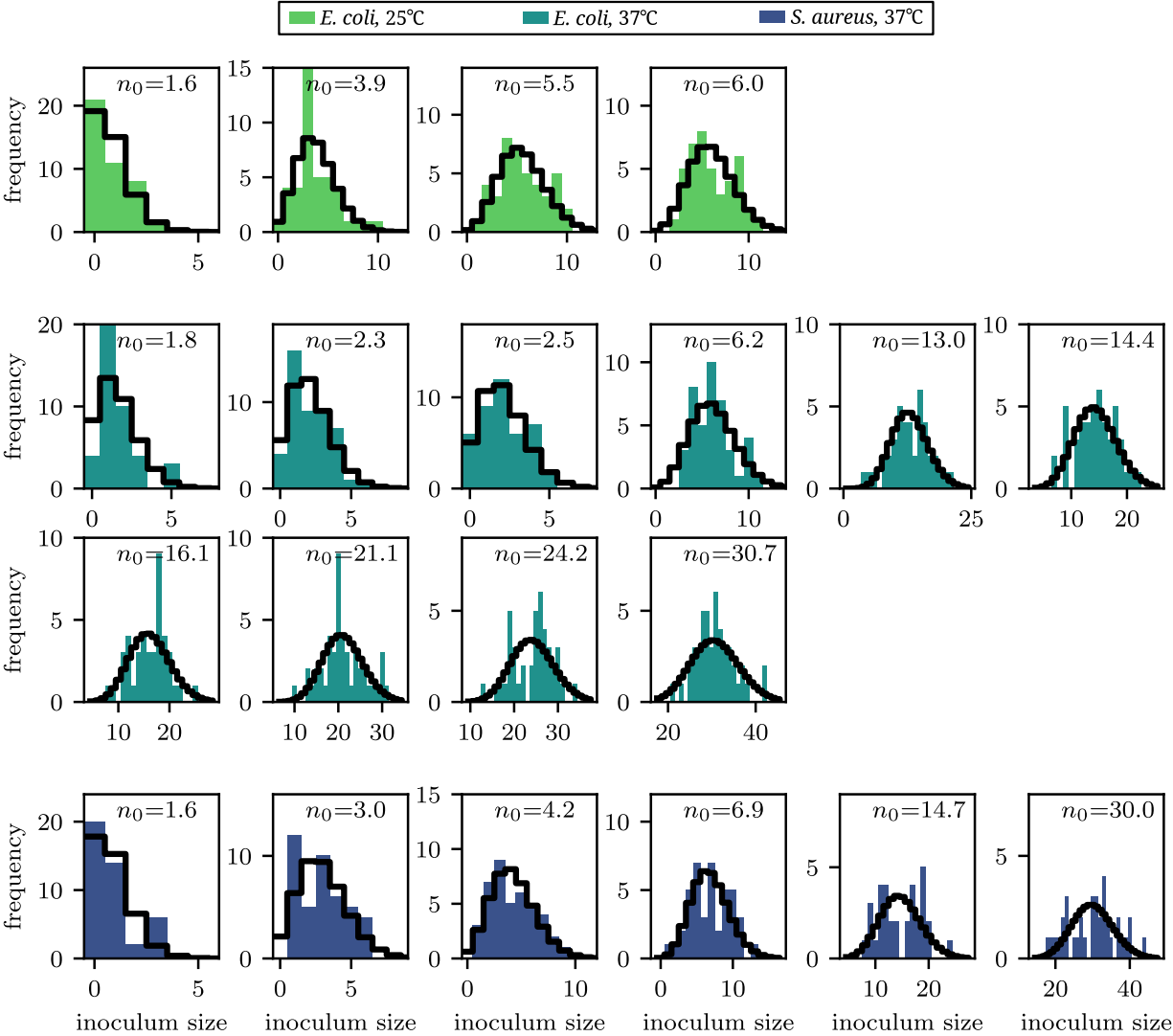


FIG. S1. **Inoculum sizes are roughly Poisson-distributed.** Distribution of inoculum sizes (filled histogram), measured by spot plating, for 20 cell cultures of varying concentrations (SI Methods). The theoretical Poisson distribution for the measured mean inoculum size is plotted in black. Spot-plating experiments were performed for each organism and growth condition, as indicated by the legend. For each distribution we report the zero-truncated mean abundance  $n_0$ , plotted in Figure 3.

## SECTION D: RELATIONSHIP BETWEEN TSD AND INOCULUM SIZE FOR POISSON-DISTRIBUTED INOCULA

Populations with Poisson-distributed inocula and deterministic exponential growth will generate a distribution of abundance trajectories. We exclusively consider trajectories with nonzero inoculum sizes. For Poisson shape parameter  $n_0$  and for positive  $k$ , the zero-truncated Poisson distribution has probability

$$P_{n_0}(k) = \frac{e^{-n_0} n_0^k}{k!(1 - e^{-n_0})} \quad (\text{S23})$$

of starting with  $k$  individuals, and zero-truncated mean  $n_0/(1 - e^{-n_0})$ . We consider deterministic population growth

$$n(t) = ke^{\mu t}, \quad (\text{S24})$$

a simplifying assumption that implies the abundance  $n(t)$  takes on non-integer values. As in Section C, the random variable

$$T(M) \equiv \frac{1}{\mu} \ln(\Omega/M) \quad (\text{S25})$$

is the first-passage time at a threshold  $\Omega$  given that the inoculum size is a random variable  $M$ . Here  $M$  is Poisson-distributed according to  $P_{n_0}$ , so the variance can be computed exactly:

$$\langle T(M)^2 \rangle - \langle T(M) \rangle^2 = \frac{e^{-n_0}}{\mu^2(1 - e^{-n_0})} \left[ \sum_{k=1}^{\infty} \frac{(\log k)^2 n_0^k}{k!} - \left( \sum_{k=1}^{\infty} \frac{n_0^k \log k}{k!} \right)^2 \frac{e^{-n_0}}{1 - e^{-n_0}} \right]. \quad (\text{S26})$$

The temporal standard deviation associated with Poisson-distributed inocula and deterministic exponential growth is therefore

$$\sqrt{\langle T(M)^2 \rangle - \langle T(M) \rangle^2} = \left\{ \frac{e^{-n_0}}{\mu^2(1 - e^{-n_0})} \left[ \sum_{k=1}^{\infty} \frac{(\log k)^2 n_0^k}{k!} - \left( \sum_{k=1}^{\infty} \frac{n_0^k \log k}{k!} \right)^2 \frac{e^{-n_0}}{1 - e^{-n_0}} \right] \right\}^{1/2}. \quad (\text{S27})$$

For large  $n_0$ , Eq. (S26) approaches  $1/(\mu^2 n_0)$ , the same as for the simple birth process. To see this, first note that for large  $n_0$  the Poisson distribution Eq. (S23) is well-approximated by a normal distribution with mean  $n_0$  and variance  $n_0$ , and the quantity  $1 - e^{-n_0}$  is well-approximated by 1. Then, following Eqs. (S21a) and (S21b), the mean first-passage time is

$$\langle T(M) \rangle = \frac{1}{\mu} \left[ \log(\Omega/n_0) + \frac{1}{2n_0} + O\left(\frac{1}{n_0^2}\right) \right], \quad (\text{S28})$$

and the variance is

$$\langle T(M)^2 \rangle - \langle T(M) \rangle^2 = \frac{1}{\mu^2 n_0} + O\left(\frac{1}{n_0^2}\right) \quad (\text{S29a})$$

$$\approx \frac{1}{\mu^2 n_0} \quad \text{for large } n_0. \quad (\text{S29b})$$

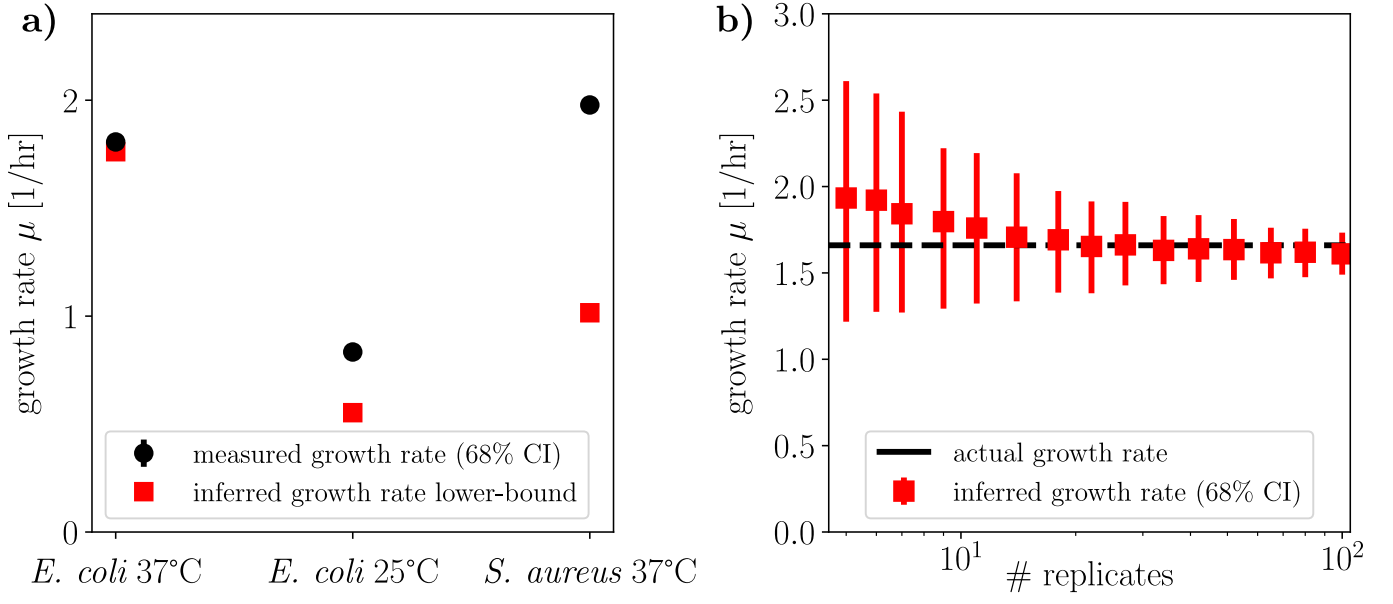


FIG. S2. **Inference of growth rates.** (a) Lower-bound for the growth rate inferred from the empirical relationship between TSD and inoculum size across organisms and growth conditions as in Eq. (12). Measured growth rate determined by computing the slope of the log-transformed optical-density time-series, as in Fig. 2c (SI Methods). Graphically, changing  $\mu$  corresponds to vertically shifting one of the red lines in the inset of Fig. 3; the lower bound here corresponds to the point at which the red line touches the convex hull of the data points. 68% confidence intervals computed with bootstrap resampling for each measured growth rate are smaller than each marker. (b) Accuracy of growth rate inference for different numbers of simulated replicate trajectories, generated by the simple birth process with inoculum size 10 (68% confidence intervals computed by subsampling from a set of 1,000 simulated trajectories, TSDs calculated with Bessel's correction). To infer the actual growth rate of 1.66/hr within 10%,  $\sim 40$  replicates are needed.

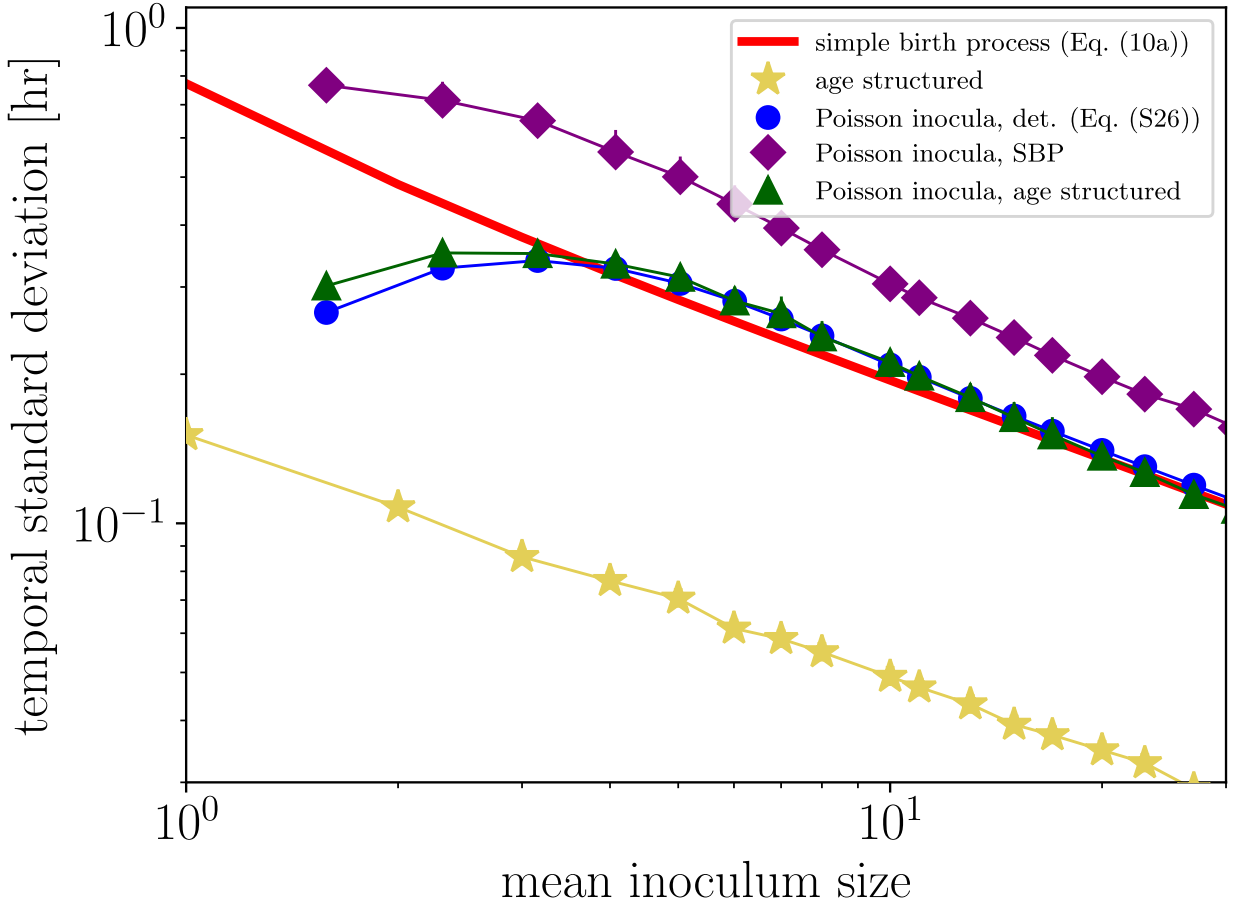


FIG. S3. **TSD as a function of mean inoculum size for five models of stochastic exponential growth.** The simple birth process (red curve) is the same as in Fig. 3. An age-structured stochastic population-growth model (gold stars) with 20 stages is simulated (10,000 replicates per inoculum size, SI Methods). A model with Poisson-distributed inocula and deterministic exponential growth (blue circles) is computed exactly [Eq. (S26)]. The simple birth process with Poisson-distributed inocula (purple diamonds) is simulated (2,000 replicates per inoculum size, SI Methods). A combined model with Poisson-distributed inocula and stochastic 20-stage population growth (green triangles) is simulated (2,000 replicates per inoculum size, Methods). The simple birth process (red) and the model with Poisson-distributed inocula and deterministic growth (blue) have similar behavior for large inoculum size, but at small inoculum sizes the simple birth process predicts more variability than the Poisson-distributed model. Error bars, which are typically smaller than the data point, show 95% confidence intervals obtained by bootstrapping (SI Methods). The growth rate  $\mu$  is 1.66/hr (25-minute average division time). For Poisson-distributed inocula, the x-axis reports the zero-truncated mean inoculum size. Lines are a guide to the eye.

## SECTION E: DETERMINISTIC AGE-STRUCTURED POPULATION GROWTH

Until this point, we have implemented population-growth models that do not resolve the structure of individual division events. Of course, organismal division is intricately choreographed and can often be broken down into discrete stages [34]. Here we examine age-structured population growth models in which division-time distributions describe the timing of division events.

Let  $n(a, t) da$  be the number of individuals aged between  $a$  and  $a + da$  at time  $t$  (where age is defined as elapsed time since previous division), and assume individuals divide with propensity  $\beta(a)$ . Population dynamics are governed by the PDE [25, 34]

$$\frac{\partial n}{\partial t} + \frac{\partial n}{\partial a} + \beta(a)n = 0, \quad (\text{S30})$$

together with the renewal condition that describes how individuals divide,

$$R(t) \equiv n(0, t) = 2 \int_0^\infty \beta(a)n(a, t) da, \quad (\text{S31})$$

and the initial condition

$$n(a, 0) = n_0(a), \quad (\text{S32})$$

where  $R(t)$  is the recruitment rate of newly divided individuals at time  $t$  (*i.e.*, the rate at which age 0 individuals enter the population, or roughly twice the growth rate of the simple birth process).

A formal solution to Eq. (S30) is

$$n(a, t) = \begin{cases} R(t-a)S(a) & \text{for } t > a \\ n_0(a-t)\tilde{S}(a, t) & \text{for } t \leq a \end{cases}, \quad (\text{S33})$$

where the ‘‘survival’’ function  $S(a) \equiv \exp[-\int_0^a \beta(u) du]$  is the proportion of individuals that survive to age  $a$  before dividing, and the modified survival function  $\tilde{S}(a, t) \equiv \exp[-\int_{a-t}^a \beta(u) du]$  is the proportion of individuals that survive to age  $a$  before dividing given that they existed and were undivided at age  $a-t$ . It is also convenient to define a normalized division-time distribution  $P_{\text{DT}}(a) \equiv \beta(a)S(a)$ . Provided no deaths occur, these functions are related according to

$$S(a) = 1 - \int_0^a P_{\text{DT}}(u) du. \quad (\text{S34})$$

From Eqs. (S31) and (S33),

$$\begin{aligned} R(t) &= 2 \underbrace{\int_0^t R(t-a)\beta(a)S(a) da}_{\text{created after } t=0} + 2 \underbrace{\int_t^\infty n_0(a-t)\beta(a)\tilde{S}(a, t) da}_{\text{from inoculum}} \\ &= 2 \int_0^t R(t-a)P_{\text{DT}}(a) da + F(t), \end{aligned} \quad (\text{S35})$$

with  $F(t) \equiv 2 \int_t^\infty n_0(a-t)\beta(a)\tilde{S}(a, t) da$  giving contributions to the recruitment rate from individuals that have not divided since inoculation.

In the special case where the inoculum consists of  $N_0$  newly divided cells,  $n_0(a) = N_0\delta(a)$  for Dirac delta function  $\delta(a)$ , and  $F(t) = 2N_0P_{\text{DT}}(t)$ . From Eqs. (S31) and (S35), the total population size is

$$N(t) = \int_0^\infty n(a, t) da = \underbrace{\int_0^t R(t-a)S(a) da}_{\text{created after } t=0} + \underbrace{\int_t^\infty n_0(a-t)\tilde{S}(a, t) da}_{\text{from inoculum}}, \quad (\text{S36})$$

which in this special case simplifies to

$$N(t) = \int_0^t R(t-a)S(a) da + N_0S(t). \quad (\text{S37})$$

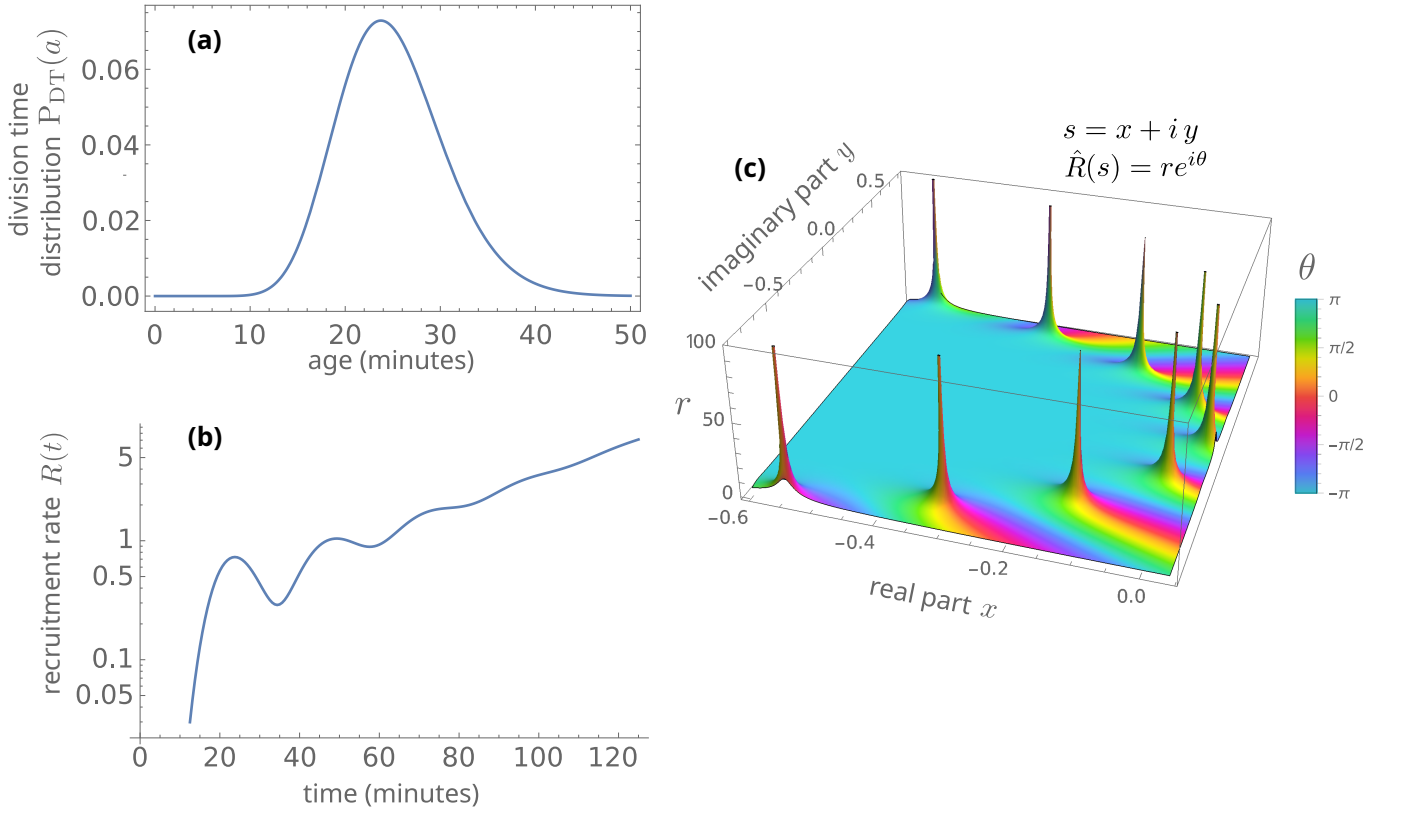


FIG. S4. **Characterization of a 20-stage population-growth model of *E. coli*.** (a) Division-time distribution for a 20-stage model given by a chi-squared distribution  $\chi^2(2k)$  with  $k = 20$  (22% coefficient of variation), linearly rescaled such that the mean division time is 25 minutes. This division-time distribution is similar to *E. coli*'s. (b) Recruitment rate  $R(t)$  contains transient oscillations that decay after a few division times. (c) Poles of the Laplace transformed recruitment rate  $\hat{R}(s)$  in an age-structured population-growth model, plotted in the complex plane. The pole with the largest real part has a positive real part and determines the long-run population-growth rate; the complex-conjugate pairs contribute to transient oscillations. The location of the three poles nearest the right-hand edge are used to compute the coherence number Eq. (S42).

The dynamics of this age-structured population therefore depend entirely on the division propensity  $\beta(a)$ , by way of the survival function  $S(a)$  and the division-time distribution  $P_{DT}(a)$ .

Laplace transforming Eq. (S35) yields

$$\hat{R}(s) = 2\hat{R}(s)\hat{P}_{DT}(s) + \hat{F}(s), \quad (\text{S38})$$

implying that

$$\hat{R}(s) = T(s)\hat{F}(s), \quad (\text{S39})$$

with  $T(s) \equiv 1/[1 - 2\hat{P}_{DT}(s)]$ . The transfer function  $T(s)$  describes the mapping in the complex  $s$ -plane from both the initial distribution of ages in the population and the division-time distribution to the solution of the dynamical system. The explicit time series for a specified initial condition is obtained by inverse Laplace transformation, a task slightly simplified in the special case where the initial population consists of newly divided cells, for which  $\hat{F}(s) = 2N_0\hat{P}_{DT}(s)$ .

Following Kendall's 1948 seminal work [3], we consider a class of age-structured models in which the division-time distribution for a  $k$ -stage population-growth model is given by a chi-squared distribution with  $2k$  degrees of freedom,  $P_{DT}(a) = \chi^2(2k)$ . The solution has the form

$$R(t) = \sum_{\text{all poles } i} c_i \exp(s_i t), \quad (\text{S40})$$

where the coefficients  $c_i$  depend on the initial age distribution, and the exponents  $s_i$  are the locations in the complex  $s$ -plane of the poles of the transfer function. The pole  $s_0$  with the largest real part determines the long-run population-

growth rate:

$$R(t) = c_0 \exp(s_0 t) \left( 1 + \sum_{i \neq 0} \frac{c_i}{c_0} \exp[(s_i - s_0)t] \right), \quad (\text{S41})$$

where the expression in parentheses approaches 1 as  $t \rightarrow \infty$ . The subdominant poles  $s_{1,2}$  are typically a complex-conjugate pair and characterize the approach to asymptotic exponential growth. Defining  $s_{1,2} \equiv \sigma \pm i\omega$  for real  $\sigma$ , the leading terms in the summation in Eq. (S41) are proportional to  $\exp[(\sigma - s_0)t] \cos(\omega t - \phi)$ , where  $\phi$  sets the phase of any transient oscillations. The period of any transient oscillations is  $2\pi/\omega$ . For all cases we explored, this period is very close to the mean division time.

The transient decays by a factor of  $e$  over a time interval  $1/(s_0 - \sigma)$ . We define the *coherence number*  $n_c$  as the number of oscillations before the transient decays by a factor of  $e$ ,

$$n_c \equiv \frac{\omega}{2\pi(s_0 - \sigma)}. \quad (\text{S42})$$

The coherence number measures the rate at which intrinsic variability desynchronizes initially synchronized division events, and therefore informs the point at which detailed non-Markovian models may be approximated by coarse-grained Markovian models like the simple birth process. Accordingly, it takes  $\log_e 10 \times n_c \approx 2.3n_c$  oscillations in order for the transient to drop to 10% of its original magnitude.

Figure S4 illustrates these concepts for the “deterministic skeleton” [35] of the stochastic 20-stage model used in Fig. S3, which describes the deterministic and incremental development of individuals until division. It shows the division-time distribution for a 20-stage population-growth model with a mean division time of 25 minutes (Fig. S4a), the leading poles (*i.e.*, those with largest real part) of the transfer function (and equivalently of  $R(s)$ ) (Fig. S4b), and the growth rate over time (Fig. S4c). The coherence number for this system is  $n_c = 1.01$ , implying that the approach to exponential growth (when the transients have dropped to 10% of their original magnitude) requires  $\sim 2.3$  cell division cycles.

We conclude that the dynamics of the 20-stage model (with initially oscillatory growth rates) approach the dynamics of the simple birth process (with growth rates proportional to population size) after a few division cycles.

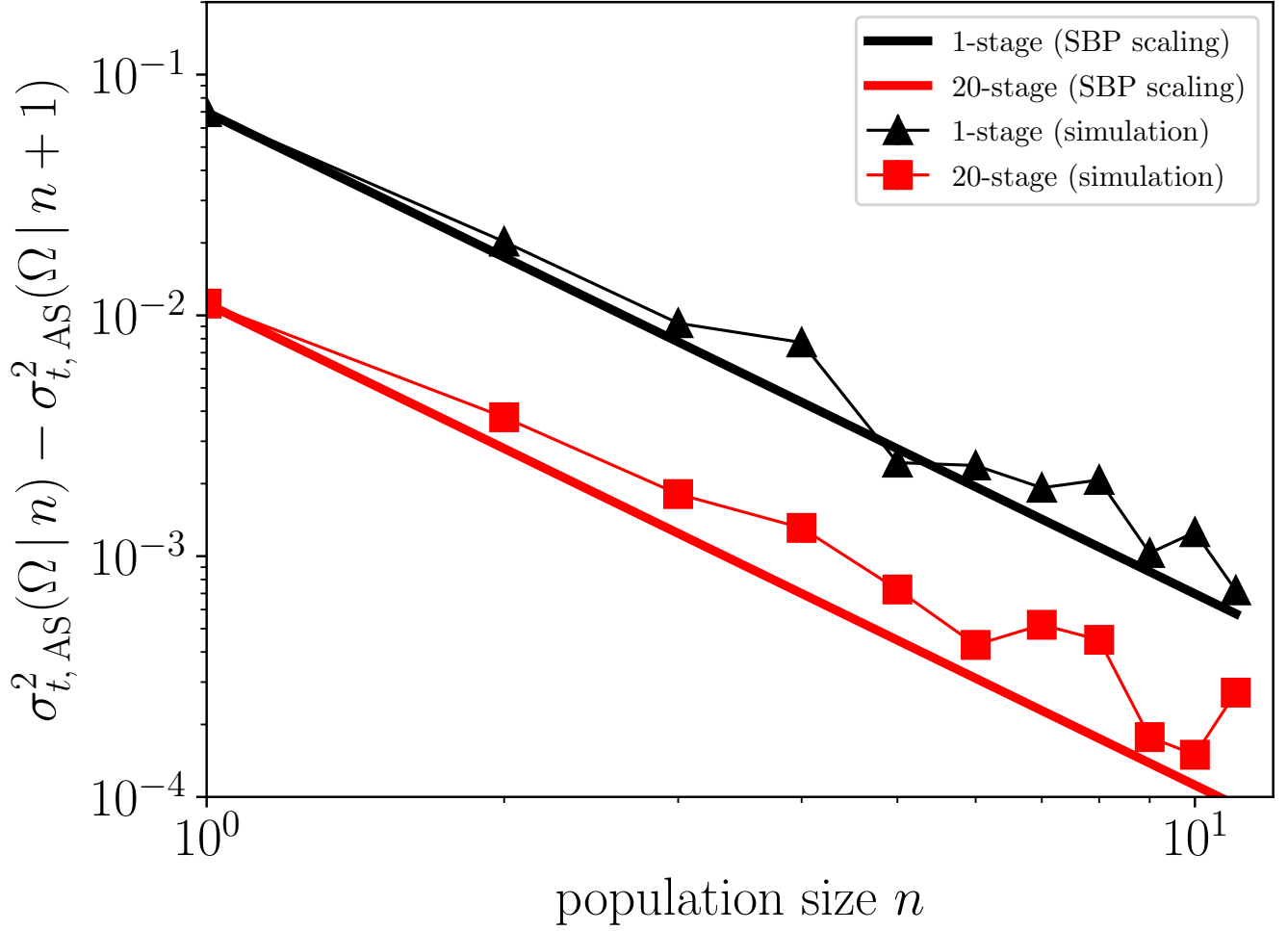


FIG. S5. **Contributions to the temporal variance across population sizes for age-structured population models.** Difference in asymptotic (large- $\Omega$ ) temporal variance  $\sigma_{t,AS}^2(\Omega | n_0)$  between inoculum sizes  $n$  and  $n + 1$  (*i.e.*, the reduction in the asymptotic temporal variance by starting with one more individual) for age-structured population growth. Points are from 1-stage and 20-stage stochastic age-structured population models (SI Methods) with 20,000 trajectories. Temporal variances are evaluated at a threshold population size  $\Omega = 500$ . 95% confidence intervals are smaller than symbols. In the simple birth process, the temporal variance [Eq. (9)] is a sum with summands that scale as  $1/n^2$ . Solid lines depict this  $1/n^2$  scaling, starting from the contribution to the asymptotic temporal variance of a single individual (graphically, a  $1/n^2$  power law starting from the  $n = 1$  data point). Thin lines are a guide to the eye.

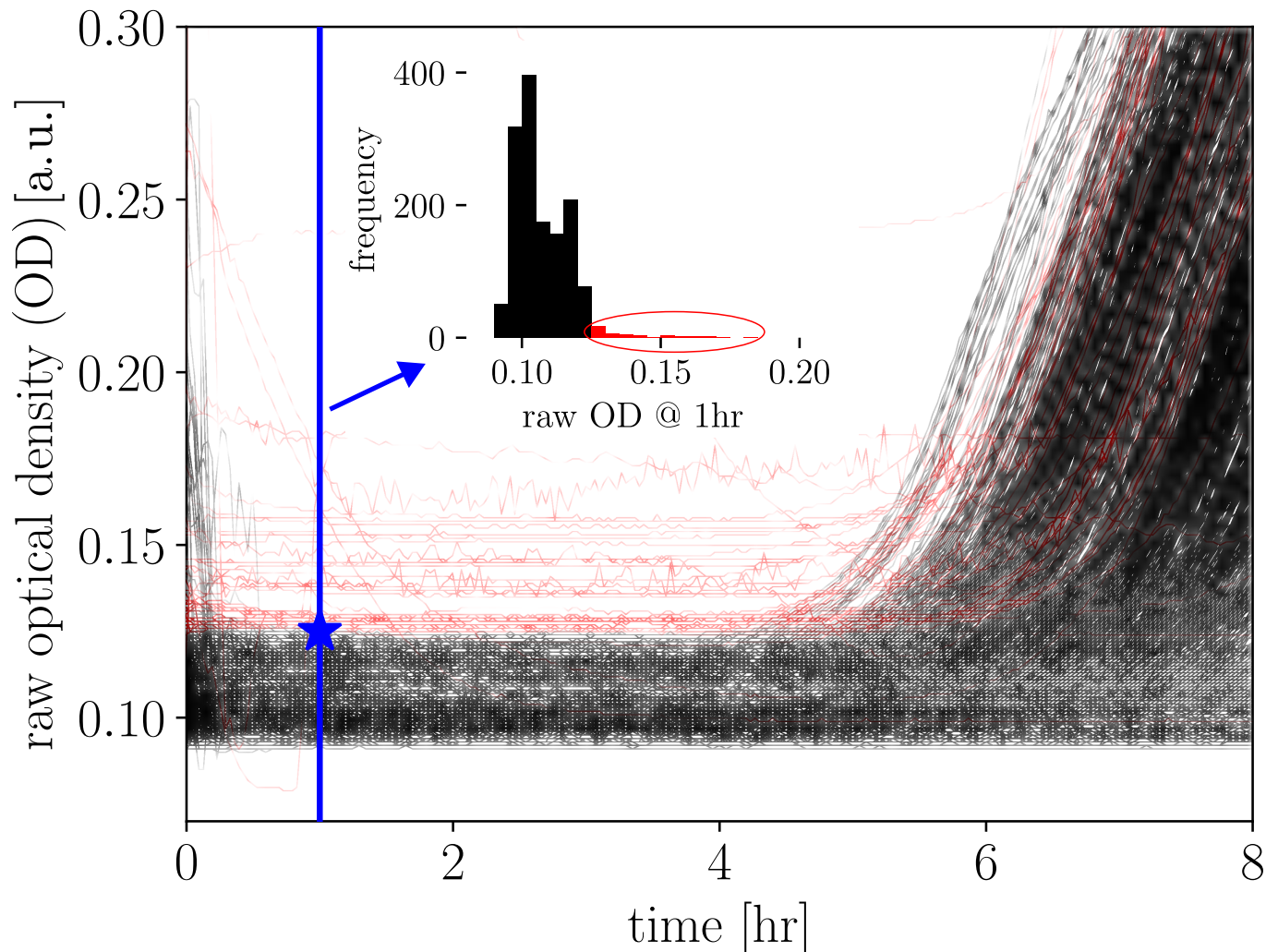


FIG. S6. **Raw optical-density measurements from all 1434 bacterial growth experiments, with 47 excluded growth curves shown in red.** Growth curves with a raw optical density (*i.e.*, before the background has been subtracted) greater than 0.125 at 1 hour post inoculation (indicated by the blue star and line) were omitted from subsequent analysis, and are indicated in red. Including every growth curve marginally increases TSDs (*e.g.*, in Fig. 3), as outliers inflate trajectory spread. (inset) Histogram of raw optical density at 1 hour post inoculation; the circled red bins indicate the  $\sim 3\%$  of trajectories that were excluded from subsequent analysis.

## METHODS

*Bacterial growth experiments.*—Either *E. coli* strain MG1655 or *S. aureus* strain NCTC 8532 was grown overnight in lysogeny broth (LB), then back diluted 1:1000 and grown to a 600nm optical density (OD600) of 0.5. At this optical density bacterial growth is in mid-log phase. Serial dilutions were performed to obtain a culture with cell concentrations between 1 and 150 CFU per  $2\mu\text{L}$ . This cell culture was subsequently used to inoculate bacterial growth experiments (*e.g.*, those in Fig. 2a,b) by pipetting  $2\mu\text{L}$  of cell culture into  $198\mu\text{L}$  of LB media. Pipetting was performed with the Rainin Pipet-Lite Multi Pipette L8-20XLS+, accurate to  $\pm 0.2\mu\text{L}$ . For each cell-culture concentration, 42 replicates were inoculated on the same 96-well plate to reduce variation, with 6 wells left as blank controls; each 96-well plate was inoculated with two sets of bacterial growth experiments. Plates were sealed with a “breathe-easy” with small holes poked in it to increase oxygen. Preparation and inoculation of 96-well plates was performed at  $24.6^\circ\text{C}$  (room temperature). Preparing each batch of experiments (consisting of three 96-well plates) took  $\sim 15$  minutes from start to finish, with inoculations for each inoculum size spanning  $\sim 3$  minutes from start to finish.

Plates were grown in a Biotek Epoch 2 plate reader for 24 hours at  $37^\circ\text{C}$  (or  $25^\circ\text{C}$ ) with continuous orbital shaking. Optical-density readings at OD600 were taken every two or three minutes. When *E. coli* was grown at  $25^\circ\text{C}$ , the time in the plate reader was extended to 48 hours. By the Beer-Lambert law, bacterial population size and OD600

are linearly correlated in the sensitivity range of the plate reader ( $>0.01$  OD) [36]. Optical-density measurements therefore serve as a proxy for bacterial population size.

*Measurement of inoculum size.*—For each concentration of cell culture, the distribution of the number of bacteria pipetted into each well of the 96-well plate (*i.e.*, the inoculum size) was inferred by spot plating an identical volume of cell culture on LB-agar plates [37]. Colonies were counted after 16 hours of growth. For each concentration of cell culture, the inoculum size is roughly Poisson-distributed (Fig. S1). The mean  $n_0$  of nonzero inoculum sizes is utilized in Figs. 2 and 3.

*Bacterial strains.*—The MG1655 strain of *E. coli* (ATCC 700926) was obtained from the Broderick lab at Johns Hopkins University. The NCTC 8532 strain of *S. aureus* (ATCC 12600) was obtained from the Saleh lab at Johns Hopkins University. Cultures were obtained by streaking from glycerol stocks onto LB-agar plates and grown for 16 hours at 37°C.

*Criteria for omission of growth curves.*—Bacterial growth curves were omitted from analysis if: (i) a well was missing an air puncture, causing anerobic growth (3/1439 replicates omitted), (ii) a well was contaminated (2/1439 replicates omitted), or (iii) raw OD600 after 1 hour of growth was above 0.125, indicating initial condensation or measurement error (47/1439 replicates omitted). In total, these exclusion criteria led to the omission of 4% (52/1439) of growth trajectories. Figure S6 shows all raw growth curves, with omitted curves in red.

*Removing optical-density background.*—The measurement background—corresponding to the light occluded by the solution (not bacteria) in a well—was subtracted from each optical-density time-series. The background was calculated as the mean optical density at time 0 for each 96-well plate, and ranged from an optical density of 0.099 to 0.121. Figures 2a and 2b show representative background-subtracted optical-density measurements. For reference, empty dry wells yield optical-density measurements of 0.005.

*Growth-rate calculation.*—For a particular bacterial growth curve, the growth rate  $\mu$  is determined by linearly regressing the log-transformed background-subtracted optical-density trajectory. Operationally, the growth rate at a given time  $t_0$  is calculated as the slope of the best-fit line for the 30-minute window centered at  $t_0$ . A single growth rate was calculated for each organism and growth condition, defined as the average growth rate across replicates and inoculum sizes evaluated at times  $t_0$  when optical-density trajectories reach threshold optical density 0.03: *E. coli* at 37°C grows at  $\mu = 1.7$ /hr, *E. coli* at 25°C grows at  $\mu = 0.8$ /hr, and *S. aureus* at 37°C grows at  $\mu = 2.0$ /hr. The growth rate is relevant for plotting TSDs in units of division time in Fig. 3, since an organism’s division time is defined as  $\ln(2)/\mu$ .

*Population-growth models.*—For each population-growth model plotted in Fig. S3, a set of integer inoculum sizes ranging from 1 to 30 were simulated. Models with Poisson-distributed inocula used this integer inoculum size as the Poisson shape parameter; the subsequent zero-truncated Poisson distribution has a larger mean inoculum size, giving rise to non-integer mean inoculum sizes. The simple birth process with exact inoculation (red) and deterministic exponential growth with Poisson-distributed inocula (blue) were computed exactly with Eqs. (10a) and (S26), respectively.

The 20-stage stochastic population-growth model with exact inoculation (gold) was simulated in an agent-based manner. Inoculated individuals were assumed to be at a random point along their division cycle, so their first division event was set to a random time uniformly drawn from  $[0, (\ln 2)/\mu]$ . Thereafter, after each division event, the two resulting individuals each randomly drew their next division time from a division-time distribution that is determined by a 20-stage growth process (in which reaching the next stage of development is a Poisson process with constant rate): specifically, this growth process yields a division-time distribution given by a chi-squared distribution  $\chi^2(40)$  [3], linearly rescaled so the mean division time was 25 minutes. Simulated TSDs were calculated at a threshold of 500 individuals.

Lastly, simple-birth-process simulations with Poisson-distributed inocula (purple) were performed by drawing 2,000 inoculum sizes from an appropriate Poisson distribution, then performing stochastic simulations using the Python function `birdepy.simulate.discrete`. For each set of simulations (gold, green, purple), 95% confidence intervals were computed by bootstrapping using the Python function `scipy.stats.bootstrap`.

*Deterministic model of age-structured growth.*—Simulations of the deterministic age-structured population-growth model displayed in Fig. S5 were performed using the Mathematica functions `TransferFunctionModel`, `TransferFunctionPoles`, and `NInverseLaplaceTransform`.

*Data and software availability.*—Raw data from bacterial growth experiments and software that can recreate main text figures are available online at GitHub: [https://github.com/erijones/intrinsic\\_variation](https://github.com/erijones/intrinsic_variation). Analyses were

performed with Python (version 3.9.7) and Mathematica (version 12.1.0.0).

- 
- [1] William Feller. Die grundlagen der volterraschen theorie des kampfes ums dasein in wahrscheinlichkeitstheoretischer behandlung. *Acta Biotheoretica*, 5(1):11–40, May 1939.
- [2] William Feller. *An Introduction to Probability Theory and Its Applications*, volume 1. Wiley, January 1968.
- [3] David G. Kendall. On the role of variable generation time in the development of a stochastic birth process. *Biometrika*, 35(3/4):316–330, 1948.
- [4] E. O. Powell. Some features of the generation times of individual bacteria. *Biometrika*, 42(1/2):16–44, 1955.
- [5] E. O. Powell. An outline of the pattern of bacterial generation times. *Microbiology*, 18(2):382–417, 1958.
- [6] W. A. O’N. Waugh. Asymptotic growth of a class of size-and-age-dependent birth processes. *Journal of Applied Probability*, 11(2):248–254, 1974.
- [7] Eberhard O. Voit and Georg Dick. Growth of cell populations with arbitrarily distributed cycle durations. I. Basic model. *Mathematical Biosciences*, 66(2):229–246, 1983.
- [8] Henry R. Hirsch and Joseph Engelberg. Decay of cell synchronization: Solutions of the cell-growth equation. *The Bulletin of Mathematical Biophysics*, 28(3):391–409, Sep 1966.
- [9] Cyril N Hinshelwood. On the chemical kinetics of autolytic systems. *Journal of the Chemical Society*, pages 745–755, 1952.
- [10] Matthew Scott and Terence Hwa. Bacterial growth laws and their applications. *Current Opinion in Biotechnology*, 22(4):559–565, 2011.
- [11] Parth Pratim Pandey, Harshant Singh, and Sanjay Jain. Exponential trajectories, cell size fluctuations, and the adder property in bacteria follow from simple chemical dynamics and division control. *Physical Review E*, 101(6):062406, 2020.
- [12] Srividya Iyer-Biswas, Gavin E Crooks, Norbert F Scherer, and Aaron R Dinner. Universality in stochastic exponential growth. *Physical Review Letters*, 113(2):028101, 2014.
- [13] Srividya Iyer-Biswas, Charles S Wright, Jonathan T Henry, Klevin Lo, Stanislav Burov, Yi Han Lin, Gavin E Crooks, Sean Crosson, Aaron R Dinner, and Norbert F Scherer. Scaling laws governing stochastic growth and division of single bacterial cells. *Proceedings of the National Academy of Sciences*, 111(45):15912–15917, 2014.
- [14] Chih-hao Hsieh, Christian S. Reiss, John R. Hunter, John R. Beddington, Robert M. May, and George Sugihara. Fishing elevates variability in the abundance of exploited species. *Nature*, 443(7113):859–862, Oct 2006.
- [15] Evgeny B. Stukalin, Ivie Aifuwa, Jin Seob Kim, Denis Wirtz, and Sean X. Sun. Age-dependent stochastic models for understanding population fluctuations in continuously cultured cells. *Journal of The Royal Society Interface*, 10(85):20130325, 2013.
- [16] Kathryn J Boor. Fluid dairy product quality and safety: looking to the future. *Journal of Dairy Science*, 84(1):1–11, 2001.
- [17] John C. Allen and Godfrey Joseph. Deterioration of pasteurized milk on storage. *Journal of Dairy Research*, 52(3):469–487, 1985.
- [18] M. Simon and A.P. Hansen. Effect of various dairy packaging materials on the shelf life and flavor of ultrapasteurized milk. *Journal of Dairy Science*, 84(4):784–791, 2001.
- [19] R.R. Petrus, C.G. Loiola, and C.A.F. Oliveira. Microbiological shelf life of pasteurized milk in bottle and pouch. *Journal of Food Science*, 75(1):M36–M40, 2010.
- [20] Jeanne-Marie Membré, Martine Kubaczka, Jonathan Dubois, and Christine Chèné. Temperature effect on *Listeria monocytogenes* growth in the event of contamination of cooked pork products. *Journal of Food Protection*, 67(3):463–469, 2004.
- [21] Food and Drug Administration. *Grade “A” Pasteurized Milk Ordinance 229*. US Department of Health and Human Services, Public Health Service, Food and Drug Administration, 1995.
- [22] Nira Richter-Dyn and Narendra S. Goel. On the extinction of a colonizing species. *Theoretical Population Biology*, 3(4):406–433, 1972.
- [23] R. C. Lewontin and D. Cohen. On population growth in a randomly varying environment. *Proceedings of the National Academy of Sciences of the United States of America*, 62(4):1056–1060, 2023/04/18/ 1969.
- [24] Michael Turelli. Random environments and stochastic calculus. *Theoretical Population Biology*, 12(2):140–178, 1977.
- [25] RM Nisbet and WSC Gurney. The formulation of age-structure models. *Mathematical Ecology: An Introduction*, pages 95–115, 1986.
- [26] Farshid Jafarpour. Cell size regulation induces sustained oscillations in the population growth rate. *Physical Review Letters*, 122:118101, Mar 2019.
- [27] Roger M Nisbet and William Gurney. *Modelling fluctuating populations: reprint of First Edition (1982)*. Blackburn Press, 2003.
- [28] Stefan W Hell, Marcus Dyba, and Stefan Jakobs. Concepts for nanoscale resolution in fluorescence microscopy. *Current Opinion in Neurobiology*, 14(5):599–609, 2004.
- [29] Nitzan Rosenfeld, Theodore J. Perkins, Uri Alon, Michael B. Elowitz, and Peter S. Swain. A fluctuation method to quantify in vivo fluorescence data. *Biophysical Journal*, 91(2):759–766, 2006.
- [30] Kiandokht Panjtan Amiri, Asa Kalish, and Shankar Mukherji. Robustness and universality in organelle size control. *Physical Review Letters*, 130:018401, Jan 2023.

- [31] Krzysztof Ptaszyński. First-passage times in renewal and nonrenewal systems. *Physical Review E*, 97(1):012127, 2018.
- [32] Donald E Knuth. *The Art of Computer Programming, Volume 1*. Bulletin of the American Mathematical Society, 1997.
- [33] Lukáš Novák and Drahomír Novák. On Taylor series expansion for statistical moments of functions of correlated random variables. *Symmetry*, 12(8), 2020.
- [34] B.L. Keyfitz and N. Keyfitz. The McKendrick partial differential equation and its uses in epidemiology and population study. *Mathematical and Computer Modelling*, 26(6):1–9, 1997.
- [35] Kevin Higgins, Alan Hastings, Jacob N Sarvela, and Louis W Botsford. Stochastic dynamics and deterministic skeletons: population behavior of dung beetle. *Science*, 276(5317):1431–1435, 1997.
- [36] Portia Mira, Pamela Yeh, and Barry G Hall. Estimating microbial population data from optical density. *PLOS ONE*, 17(10):e0276040, 2022.
- [37] AF Gaudy, Jr, F Abu-Niaaj, and ET Gaudy. Statistical study of the spot-plate technique for viable-cell counts. *Applied Microbiology*, 11(4):305–309, 1963.